

Wideband Second-Order Adjoint Sensitivity Analysis Exploiting TLM

Mohamed H. Negm, *Student Member, IEEE*, Mohamed H. Bakr, *Senior Member, IEEE*, Osman S. Ahmed, *Member, IEEE*, Natalia K. Nikolova, *Fellow, IEEE*, and John W. Bandler, *Life Fellow, IEEE*

Abstract—We present, for the first time, an efficient adjoint variable method (AVM) for estimating second-order sensitivities exploiting time-domain transmission-line modeling. For a structure with n designable parameters, the complete Hessian matrix of any desired objective function is estimated using n extra simulations as compared to $O(n^2)$ using the traditional finite-difference approaches. Our approach is illustrated through estimating the second-order sensitivities for energy functions and scattering parameter with respect to dimensions and material properties of metallic and dielectric discontinuities. The results achieved using our AVM approach are verified using the expensive finite-difference approaches.

Index Terms—Adjoint variable method (AVM), electromagnetic (EM) modeling, optimization, transmission-line modeling (TLM).

I. INTRODUCTION

SENSITIVITY analysis has attracted great interest in microwave circuit design. It has wide applications in yield analysis, tolerance analysis, and gradient-based optimization [1]. Full-wave numerical electromagnetic (EM) solvers can solve complex microwave and antenna structures [2]. Using finite-difference approximations, these solvers supply first- and second-order sensitivities of the desired responses using repeated simulations with perturbed parameters. First-order sensitivities are estimated using $O(n)$ extra simulations, where n is the number of parameters. Second-order sensitivities require $O(n^2)$ extra simulations. As the complexity of the problem increases, the required computation overhead becomes prohibitive despite the acceleration of computing speeds. As a result, special focus is put on reducing the number of simulations required for sensitivity analysis.

The adjoint variable method (AVM) aims at efficiently estimating the sensitivities of a desired objective function or response. Using at most one extra adjoint simulation, the first-order sensitivities of the objective function are estimated with respect to all parameters regardless of their number. First-order AVM has been successfully implemented in time-

and frequency-domain EM solvers [3]–[8]. These methods include the finite-element method (FEM) [4], finite-element time-domain (FETD) [3], method of moments (MoM) [8], frequency-domain transmission-line modeling (FD-TLM) [5], time-domain transmission-line modeling (TD-TLM) [6], and finite-difference time-domain (FDTD) [7]. The AVM is already utilized to estimate the scattering parameters (S -parameters) first-order sensitivities in commercial solvers [9], [10].

Second-order (Hessian) sensitivity information are known to accelerate the convergence of the optimization algorithms [11], [12]. These sensitivities are, however, very expensive to calculate. Different approaches to approximate the second-order sensitivities have been developed through iterative approaches, e.g., [12]–[14].

The AVM approach has been extended to estimate second-order and higher order adjoint sensitivities in fluid dynamics [15], [16] and circuit applications [17]–[20]. The second-order derivatives of the S -parameters were computed based on the adjoint network method (ANM) for microwave filters with respect to all design parameters. This approach is applicable only to narrowband frequency-domain solvers.

In this paper, we extend our previous work [21] on AVM to estimate wideband time-domain-based second-order derivatives of arbitrary responses, to include scattering parameters and 3-D full-wave simulations. Our approach is illustrated with TD-TLM [22]. Using only n extra simulations, all n^2 components of the Hessian matrix are estimated. First-order sensitivities are also estimated as a by-product of our algorithm. It follows that an accurate second-order Taylor's expansion of the response is achieved in an efficient way.

This paper is organized as follows. Section II gives a brief review of the TLM method and the AVM theory for estimating first-order sensitivities. Section III presents a detailed derivation of the AVM theory for estimating second-order sensitivities. Section IV explains the practical implementation of the algorithm. Section V illustrates the theory through a number of examples. We finally conclude in Section VI.

II. FIRST-ORDER AVM

A. TLM Method

The transmission-line matrix method models the propagation of EM waves in the time domain [23], [22], where both time and space are discretized. The computational domain is modeled by a grid of nodes connected together with transmission-line links. The scattering of voltage impulses over these links models the propagation of EM waves. The electric and magnetic fields are

Manuscript received July 18, 2013; revised December 17, 2013; accepted December 18, 2013. Date of publication January 21, 2014; date of current version March 03, 2014.

M. H. Negm, M. H. Bakr, N. K. Nikolova, and J. W. Bandler are with the Department of Electrical and Computer Engineering, McMaster University, Hamilton, ON, L8S 1J4 Canada (e-mail: negmmh@mcmaster.ca).

O. S. Ahmed is with the The Edward S. Rogers Sr. Department of Electrical and Computer Engineering, University of Toronto, Toronto, ON, Canada M5S 3G4.

Color versions of one or more of the figures in this paper are available online at <http://ieeexplore.ieee.org>.

Digital Object Identifier 10.1109/TMTT.2014.2299521

linear functions of the voltage impulses incident on the transmission lines. An impulse incident on one of these transmission lines follows a sequence of scattering and connection steps. The scattering and connection steps for incident impulses on all transmission lines are governed by

$$\mathbf{V}_{k+1} = \mathbf{C}\mathbf{S}\mathbf{V}_k + \mathbf{V}_k^s \quad (1)$$

where \mathbf{V}_k is the vector of incident impulses for all nodes at the k th time step. The matrix \mathbf{S} is a block diagonal matrix of the whole domain. \mathbf{C} is the connection matrix that describes how the reflected impulses are connected to their neighboring nodes/boundaries. \mathbf{V}_k^s is the vector of the excitation source at the k th time step. Even though (1) is used to mathematically express the scattering and connection steps, the actual implementation does not perform matrix multiplication on the large matrices \mathbf{S} and \mathbf{C} . The scattering and connection steps are carried out on a cell-by-cell basis.

B. First-Order AVM

An EM design problem can be formulated as a minimization problem [6]

$$\mathbf{x}^* = \arg \left\{ \min_{\mathbf{x}} F(\mathbf{x}, \mathbf{R}(\mathbf{x})) \right\} \quad (2)$$

where $\mathbf{x} \in \mathbb{R}^n$ is the vector of all design parameters, $\mathbf{R}(\mathbf{x})$ is the vector of EM responses, F is the objective function to be minimized, and \mathbf{x}^* is the vector of optimal design parameters. Solving (2) with a gradient-based optimization algorithm requires the first-order sensitivities (response gradient). A faster convergence is achieved when the second-order sensitivities (Hessian) information is available.

One of the most efficient gradient estimation techniques is the AVM. Using at most one extra simulation, all components of the response gradient vector are estimated regardless of their number. The AVM implementation in the case of TLM simulations has been reported in [6] and [24]–[27].

The AVM considers an objective function of the form

$$F(\mathbf{x}, \mathbf{V}) = \int_0^{T_m} \Psi(\mathbf{x}, \mathbf{V}) dt \quad (3)$$

where \mathbf{V} is the vector of TLM link incident voltages and T_m is the simulation time. The sensitivity of F with respect to the i th design parameter, \mathbf{x}_i , $i = 1, 2, \dots, n$, is given by [6]

$$\frac{\partial F}{\partial \mathbf{x}_i} = -\Delta t \sum_k \boldsymbol{\lambda}_k^T \frac{\Delta \mathbf{A}}{\Delta \mathbf{x}_i} \mathbf{V}_k \quad (4)$$

where $\boldsymbol{\lambda}$ is the adjoint variable vector calculated using the adjoint simulation [6] and k is the time-step index. The simulation runs backward in time and is given by

$$\boldsymbol{\lambda}_{k-1} = \mathbf{S}^T \mathbf{C}^T \boldsymbol{\lambda}_k - \mathbf{V}_k^{s,\lambda} \quad \boldsymbol{\lambda}(T_m) = \mathbf{0} \quad (5)$$

where $\mathbf{V}_k^{s,\lambda}$ is the adjoint excitation ($\mathbf{V}_k^{s,\lambda} = \Delta t (\partial \Psi / \partial \mathbf{V})_{t=\Delta t}$). The matrix $\Delta \mathbf{A}_i$ is the net change in the system matrix due to perturbation of the variable \mathbf{x}_i .

The system matrix \mathbf{A} of the TLM problem is defined for a band-limited excitation and sufficiently small time step, Δt , by utilizing a first-order Taylor's expansion on (1) to obtain [6]

$$\mathbf{V}_k + \left(\frac{\partial \mathbf{V}}{\partial t} \right)_k \Delta t \approx \mathbf{C}\mathbf{S}\mathbf{V}_k + \mathbf{V}_k^s \quad (6)$$

Reorganizing (6), we have the temporal first-order differential equation governing the incident impulses

$$\left(\frac{\partial \mathbf{V}}{\partial t} \right)_k \approx \mathbf{A}(\mathbf{x})\mathbf{V} + \frac{\mathbf{V}_k^s}{\Delta t} \quad (7)$$

where

$$\mathbf{A} = (\mathbf{C}\mathbf{S} - \mathbf{I}) / \Delta t. \quad (8)$$

The matrix $\Delta \mathbf{A} \forall i$ has very few nonzero components corresponding to the perturbed nodes in the computational domain. The sparsity in $\Delta \mathbf{A}_i$ allows for storing a reduced number of components of the vectors \mathbf{V} and $\boldsymbol{\lambda}$ at all time steps.

III. THEORY OF SECOND-ORDER AVM

The second-order derivative is traditionally calculated using finite-difference techniques and gradient-based approximations. The central finite difference (CFD) general expression for the second derivative is [28]

$$\frac{\partial^2 F}{\partial x_i \partial x_j} \approx \left(\begin{array}{c} F(x_i + \Delta x_i, x_j + \Delta x_j) \\ -F(x_i + \Delta x_i, x_j - \Delta x_j) \\ -F(x_i - \Delta x_i, x_j + \Delta x_j) \\ +F(x_i - \Delta x_i, x_j - \Delta x_j) \end{array} \right) / 4\Delta x_i \Delta x_j. \quad (9)$$

Calculating all n^2 components of the symmetric Hessian matrix requires $O(n^2)$ extra simulations. This cost is, for most practical problems, computationally prohibitive.

Here, we give a detailed derivation of an AVM approach to second-order sensitivity estimation. Assuming an objective function of the form (3), we consider two parameters x_i and x_j , where $i \neq j$. The first-order differential equation (7) is rewritten as a function of two distinct parameters as [6]

$$\frac{\partial \mathbf{V}(x_i, x_j)}{\partial t} = \mathbf{A}(x_i, x_j)\mathbf{V}(x_i, x_j) + \frac{\mathbf{V}_s}{\Delta t}. \quad (10)$$

Perturbing only in the direction of x_i by Δx_i , we get the perturbed differential equation

$$\frac{\partial \mathbf{V}(x_i + \Delta x_i, x_j)}{\partial t} = \mathbf{A}(x_i + \Delta x_i, x_j)\mathbf{V}(x_i + \Delta x_i, x_j) + \frac{\mathbf{V}_s}{\Delta t}. \quad (11)$$

To simplify the notation, we write $\mathbf{Z}(x + \Delta x, y)$ as $\mathbf{Z}(x^+, y)$ in all subsequent equations such that $\mathbf{Z} \equiv \{\mathbf{A}, \mathbf{V}\}$. Subtracting (10) from (11), we get

$$\frac{\partial \mathbf{V}(x_i^+, x_j)}{\partial t} - \frac{\partial \mathbf{V}(x_i, x_j)}{\partial t} = \mathbf{A}(x_i^+, x_j)\mathbf{V}(x_i^+, x_j) - \mathbf{A}(x_i, x_j)\mathbf{V}(x_i, x_j). \quad (12)$$

Dividing both sides of (12) by Δx_i and using the chain rule of differentiation, we get the second-order differential equation

$$\frac{\partial^2 \mathbf{V}(x_i, x_j)}{\partial x_i \partial t} \approx \left[\frac{\mathbf{A}(x_i^+, x_j) - \mathbf{A}(x_i, x_j)}{\Delta x_i} \right] \mathbf{V}(x_i, x_j) + \mathbf{A}(x_i^+, x_j) \frac{\partial \mathbf{V}(x_i, x_j)}{\partial x_i}. \quad (13)$$

Furthermore, perturbing the parameter x_j in (13) by Δx_j , we have

$$\frac{\partial^2 \mathbf{V}(x_i, x_j^+)}{\partial x_i \partial t} \approx \left[\frac{\mathbf{A}(x_i^+, x_j^+) - \mathbf{A}(x_i, x_j^+)}{\Delta x_i} \right] \mathbf{V}(x_i, x_j^+) + \mathbf{A}(x_i^+, x_j^+) \frac{\partial \mathbf{V}(x_i, x_j^+)}{\partial x_i}. \quad (14)$$

Subtracting (13) from (14) and dividing by Δx_j , the following third-order differential equation is obtained:

$$\frac{\partial^3 \mathbf{V}}{\partial x_i \partial x_j \partial t} = \frac{\mathbf{T}_1}{\Delta x_i \Delta x_j} \mathbf{V} + \frac{\mathbf{T}_2}{\Delta x_i} \frac{\partial \mathbf{V}}{\partial x_j} + \frac{\mathbf{T}_3}{\Delta x_j} \frac{\partial \mathbf{V}}{\partial x_i} + \mathbf{A}(x_i^+, x_j^+) \frac{\partial^2 \mathbf{V}}{\partial x_i \partial x_j} \quad (15)$$

where

$$\begin{aligned} \mathbf{T}_1 &= \mathbf{A}(x_i^+, x_j^+) - \mathbf{A}(x_i, x_j^+) - \mathbf{A}(x_i^+, x_j) + \mathbf{A}(x_i, x_j) \\ \mathbf{T}_2 &= \mathbf{A}(x_i^+, x_j^+) - \mathbf{A}(x_i, x_j^+) \end{aligned}$$

and

$$\mathbf{T}_3 = \mathbf{A}(x_i^+, x_j^+) - \mathbf{A}(x_i^+, x_j). \quad (16)$$

The corresponding adjoint system is defined using (15). Multiplying (15) by an arbitrary variable vector, $\boldsymbol{\lambda}$, and integrating over time by parts, one gets

$$\begin{aligned} \int_0^{T_m} \left(\frac{d\boldsymbol{\lambda}^T}{dt} + \boldsymbol{\lambda}^T \mathbf{A}(x_i^+, x_j^+) \right) \frac{\partial^2 \mathbf{V}}{\partial x_i \partial x_j} dt \\ = - \int_0^{T_m} \boldsymbol{\lambda}^T \left(\frac{\mathbf{T}_1}{\Delta x_i \Delta x_j} \mathbf{V} + \frac{\mathbf{T}_2}{\Delta x_i} \frac{\partial \mathbf{V}}{\partial x_j} + \frac{\mathbf{T}_3}{\Delta x_j} \frac{\partial \mathbf{V}}{\partial x_i} \right) dt. \end{aligned} \quad (17)$$

It can be shown that the second-order derivative of the objective function in (3) with respect to any two parameters x_i and x_j ($i \neq j$) is given by

$$\frac{\partial^2 F}{\partial x_i \partial x_j} = \frac{\partial^{(e)2} F}{\partial x_i \partial x_j} + \int_0^{T_m} \left[\left(\frac{\partial \Psi}{\partial \mathbf{V}} \right)^T \cdot \frac{\partial^2 \mathbf{V}}{\partial x_i \partial x_j} + \left(\frac{\partial \mathbf{V}}{\partial x_j} \right)^T \cdot \left(\frac{\partial^2 \Psi}{\partial \mathbf{V}^2} \right)^T \cdot \frac{\partial \mathbf{V}}{\partial x_i} \right] dt. \quad (18)$$

Here, $\partial^{(e)2} F / \partial x_i \partial x_j$ is the explicit second derivative, which is equal to zero in most practical objective functions. Comparing the first term of the integral in (18) with the left-hand side of (17), we have the following equation for the adjoint TLM problem:

$$\frac{d\boldsymbol{\lambda}^T}{dt} + \boldsymbol{\lambda}^T \mathbf{A}(x_i^+, x_j^+) = \left(\frac{\partial \Psi}{\partial \mathbf{V}} \right)^T. \quad (19)$$

By using the definition of the system matrix \mathbf{A} in (8) and rearranging, we obtain the following equation governing the adjoint system:

$$\boldsymbol{\lambda}_{k-1} = \mathbf{S}^\lambda \mathbf{C}^\lambda \boldsymbol{\lambda}_k - \mathbf{V}_k^{s,\lambda} \quad \boldsymbol{\lambda}(T_m) = \mathbf{0} \quad (20)$$

where $\mathbf{V}_k^{s,\lambda} = \Delta t (\partial \Psi / \partial \mathbf{V})^T$ is the adjoint excitation. To avoid carrying out more than one adjoint problem, the perturbed scattering and connection matrices $\mathbf{S}(x_i^+, x_j^+)$ and $\mathbf{C}(x_i^+, x_j^+)$ are approximated with the original matrices (\mathbf{S} and \mathbf{C} , respectively). This approximation is valid as long as the perturbations Δx_i and Δx_j are small enough. The adjoint expression in (20) is the same as the adjoint expression for the first-order AVM sensitivity in (5). This implies that the same adjoint simulation is used to extract both the first- and the second-order response derivatives. Using (17) and (18), the adjoint variable expression for the second-order sensitivity is given by

$$\begin{aligned} \frac{\partial^2 F}{\partial x_i \partial x_j} = \int_0^{T_m} \left(\frac{\partial \mathbf{V}}{\partial x_j} \right)^T \left(\frac{\partial^2 \Psi}{\partial \mathbf{V}^2} \right)^T \frac{\partial \mathbf{V}}{\partial x_i} \\ - \boldsymbol{\lambda}^T \left(\frac{\mathbf{T}_1}{\Delta x_i \Delta x_j} \mathbf{V} + \frac{\mathbf{T}_2}{\Delta x_i} \frac{\partial \mathbf{V}}{\partial x_j} + \frac{\mathbf{T}_3}{\Delta x_j} \frac{\partial \mathbf{V}}{\partial x_i} \right) dt. \end{aligned} \quad (21)$$

In addition to the vector of original impulses \mathbf{V} obtained using (1) and the adjoint response, $\boldsymbol{\lambda}$, obtained using (20), the vectors $\partial \mathbf{V} / \partial x_i$ and $\partial \mathbf{V} / \partial x_j$ are also required. These can be obtained through perturbed simulations. To calculate all components of the Hessian matrix, n extra simulations are thus needed.

It is noteworthy from the above derivation that positive perturbation is assumed for both parameters x_i and x_j in (16). Other perturbations can be assumed such as negative perturbation of both parameters $\{x_i^-, x_j^-\}$ or a combination of positive and negative perturbations $\{x_i^+, x_j^-\}$ and $\{x_i^-, x_j^+\}$. In the case of a single parameter ($i = j$), central perturbation is assumed $\{x_i^+, x_i^-\}$. This will accordingly affect the adjoint system matrix in (19) depending on the direction of perturbation.

IV. ALGORITHM IMPLEMENTATION

Similar to the first-order AVM approach, the second-order AVM requires storing the field information at certain locations in the computational domain corresponding to the respective parameter change [6]. This is achieved through the following steps: 1) parameterization; 2) original analysis; 3) adjoint analysis; and 4) sensitivity estimation. In the parameterization phase, the system matrix (8) is defined for the nominal and perturbed domains. The changes in the system matrix required for calculating the terms \mathbf{T}_1 , \mathbf{T}_2 , and \mathbf{T}_3 in (16) are determined. These three sparse matrices have a few nonzero elements corresponding to the perturbed subsets of the computational domain. We assume in our implementation that the change in the system matrix is represented by a change in the scattering matrix, $\mathbf{S}(\mathbf{x})$, while the connection matrix, $\mathbf{C}(\mathbf{x})$, is kept unchanged. The local changes in the electric conductivity, $\sigma(\mathbf{x})$, and relative permittivity, $\varepsilon_r(\mathbf{x})$, that may occur due to a change in any of the design parameters, are reflected in changes in the scattering matrix. Fig. 1(a)–(d) illustrates

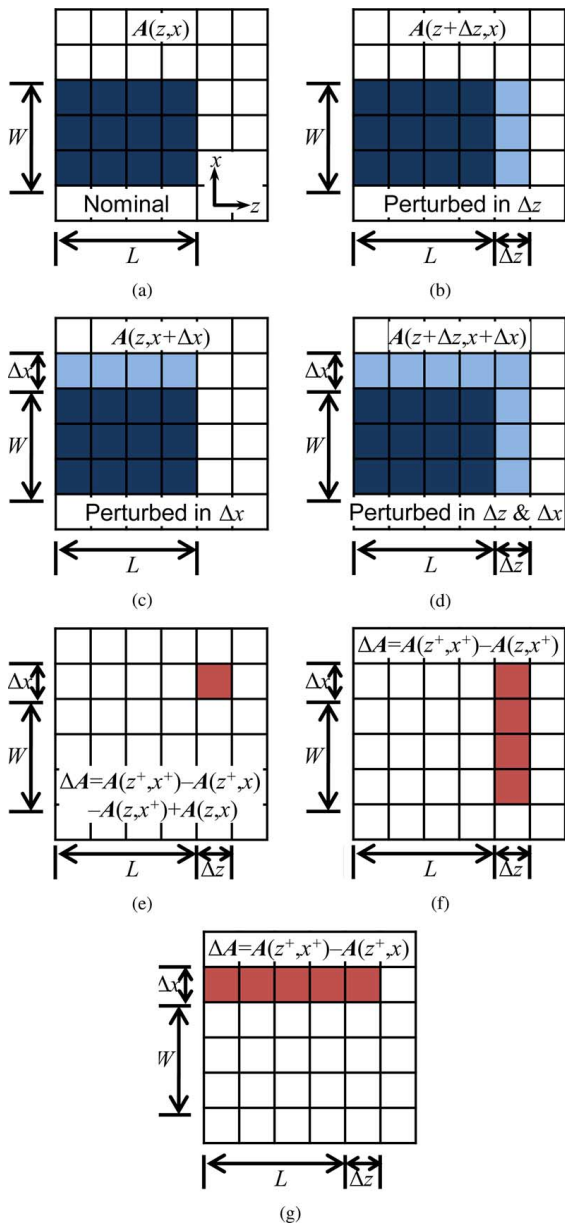


Fig. 1. Illustration of system matrix perturbations for an arbitrary discontinuity in TLM domain. (a) Nominal structure, (b) perturbation in the parameter L by Δz , (c) perturbation in the parameter W by Δx , (d) perturbations in both L and W , (e) change T_1 , (f) change T_2 , and (g) change T_3 in (16).

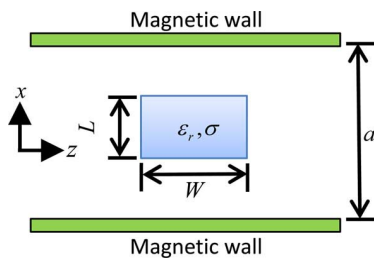


Fig. 2. TEM-mode parallel-plate waveguide loaded with a rectangular dielectric discontinuity. The waveguide has a width $a = 30$ mm and length $2a = 60$ mm. The TLM cell is $\Delta l = 1.0$ mm. The dielectric has $\epsilon_r = 1.5$, and $\sigma = 1.0 \text{ S} \cdot \text{m}^{-1}$.

this concept. Changing the length (L) or width (W) of the shown discontinuity results in changing material properties

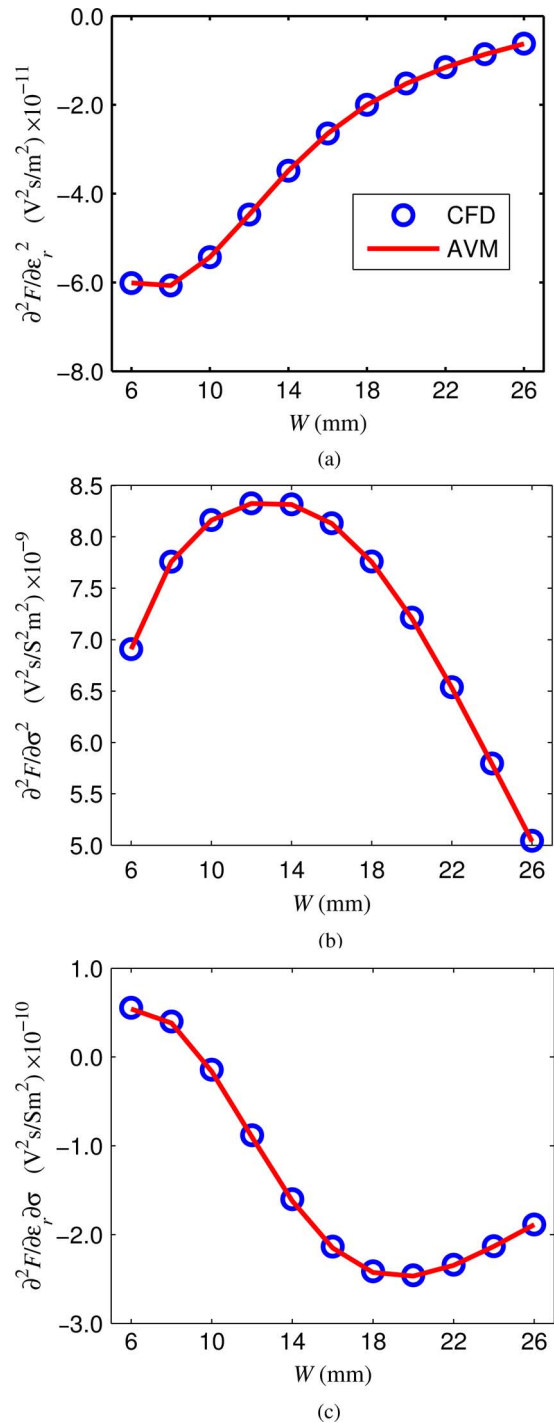


Fig. 3. Second-order sensitivities of the objective function in (22) with respect to ϵ_r and σ of the rectangular dielectric discontinuity shown in Fig. 2. The sensitivities are estimated using CFD (\circ) and AVM ($-$) for different discontinuity widths.

for certain subsets of the computational domain. The nonzero components of the matrices T_1 , T_2 , and T_3 are determined by subtracting these subsets from one another, as shown in Fig. 1(e)–(g).

In the original analysis, the forward TLM simulation in (1) is executed. The first three terms on the right-hand side of (15) are computed at the nonzero links and stored at all the time steps. These terms are weighted summations of the incident impulses

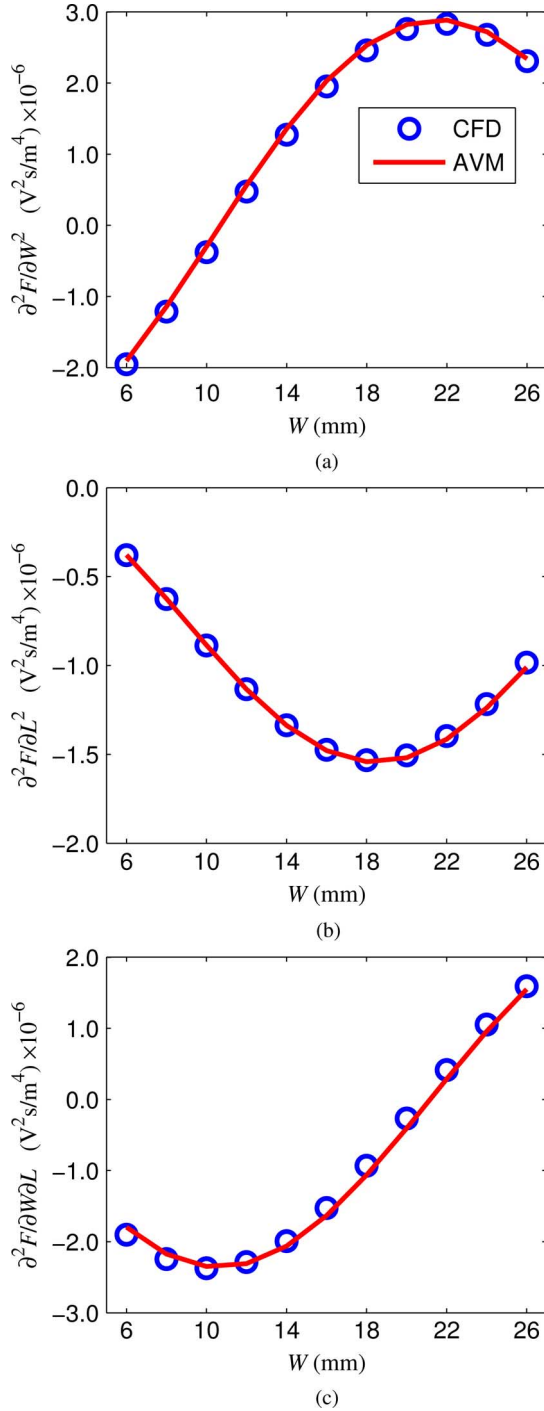


Fig. 4. Second-order sensitivities of the objective function in (22) with respect to the length, L , and width, W , of the rectangular dielectric discontinuity shown in Fig. 2. The sensitivities are estimated using CFD (○) and AVM (—) for different discontinuity widths.

and their derivatives. The adjoint excitation in (20) is also determined at every time step.

In the third step, the adjoint analysis in (20) is executed. The adjoint field components are computed at the locations corresponding to the nonzero links in the original system. To reduce the memory overhead, the adjoint field values are not stored, but rather are multiplied on-the-fly by the terms in (15) [see also (21)] during the adjoint simulation for each parameter [29].

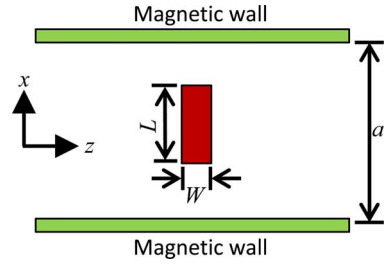


Fig. 5. 2-D parallel-plate waveguide with a metallic inductive obstacle centered in the middle. The waveguide has a width $a = 60$ mm and length $2a = 120$ mm. The TLM cell is $\Delta l = 1.0$ mm. The obstacle width is fixed at $W = 6.0$ mm.

V. NUMERICAL EXAMPLES

The theory presented in Sections III and IV is validated through a number of numerical examples. These examples utilize different types of objective functions. All examples are simulated using our in-house TLM solver written in MATLAB R2010a, which runs on an Intel Xeon CPU 5160 at 3.0 GHz and 16.0 GB of RAM.

A. Rectangular Dielectric Discontinuity

Our algorithm is applied to the sensitivity analysis of a TEM-mode parallel-plate waveguide loaded with a rectangular dielectric discontinuity (see Fig. 2). The relative permittivity, ϵ_r , and conductivity, σ , are 1.5 and $1.0 \text{ S} \cdot \text{m}^{-1}$, respectively. The vector of design parameters is defined to be $\mathbf{x} = [\epsilon_r, \sigma, W, L]^T$.

The waveguide has a width of $a = 30$ mm and length of $2a = 60$ mm. The dielectric discontinuity has a constant length of $L = 16$ mm. The sensitivities are estimated for a sweep of dielectric widths, $W = 6, 8, 10, \dots, 26$ mm. The domain is discretized into square TLM cells of size $\Delta l = 1.0$ mm. The ports are modeled with wideband absorbing boundary condition for TEM waves propagating in free space with an impulse reflection coefficient of -0.17157 . The domain is excited with a Gaussian-modulated sine wave with a center frequency at $f_0 = 3.0$ GHz and a bandwidth of $\Delta f = 2.0$ GHz, injected from the left port of the waveguide. The objective function is defined by the energy

$$F(\mathbf{x}, \mathbf{V}) = \frac{\int_0^{T_m} \int_{\Omega} e_y^2 dx dt}{\Delta l} \quad (22)$$

where the observation domain, Ω , is the last column of nodes at the output port. e_y is the y component of the electric field at each node. The second-order sensitivities of (22) with respect to the constitutive parameters ($\partial^2 F / \partial \epsilon_r^2$, $\partial^2 F / \partial \epsilon_r \partial \sigma$, and $\partial^2 F / \partial \sigma^2$) and the shape parameters ($\partial^2 F / \partial W^2$, $\partial^2 F / \partial L^2$, and $\partial^2 F / \partial W \partial L$) are shown in Figs. 3 and 4, respectively. The results achieved using our second-order AVM match those obtained using the accurate, but time-intensive CFD approximation. The CFD requires 17 independent simulations, while our approach requires only six independent simulations, a reduction of 64%.

B. Inductive Obstacle

We consider an inductive obstacle in a parallel-plate waveguide, as shown in Fig. 5. The waveguide has a width of $a =$

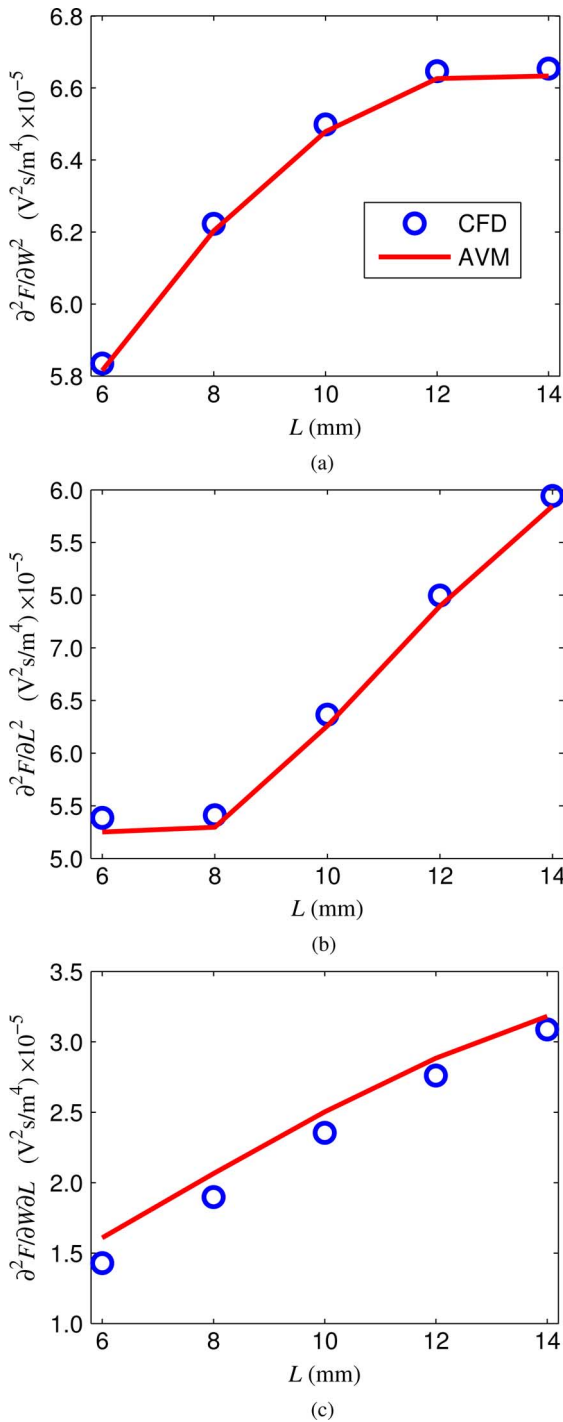


Fig. 6. Second-order sensitivities of the objective function in (22) with respect to length, L , and width, W , of the inductive obstacle shown in Fig. 5. The sensitivities are estimated using CFD (\circ) and AVM ($—$), at different obstacle lengths.

60 mm and a length of 62 mm. The metallic obstacle is centered in the middle of the waveguide with a fixed width, $W = 6.0$ mm. A square TLM cell of size $\Delta l = 1.0$ mm is utilized. The vector of design parameters is $\mathbf{x} = [W L]^T$. The waveguide is excited with a Gaussian-modulated sine wave centered at $f_0 = 2.0$ GHz and a bandwidth of $\Delta f = 2.0$ GHz. The derivatives $\partial^2 F / \partial W^2$, $\partial^2 F / \partial L^2$, and $\partial^2 F / \partial W \partial L$ of the energy function in (22) are estimated at different obstacle lengths,

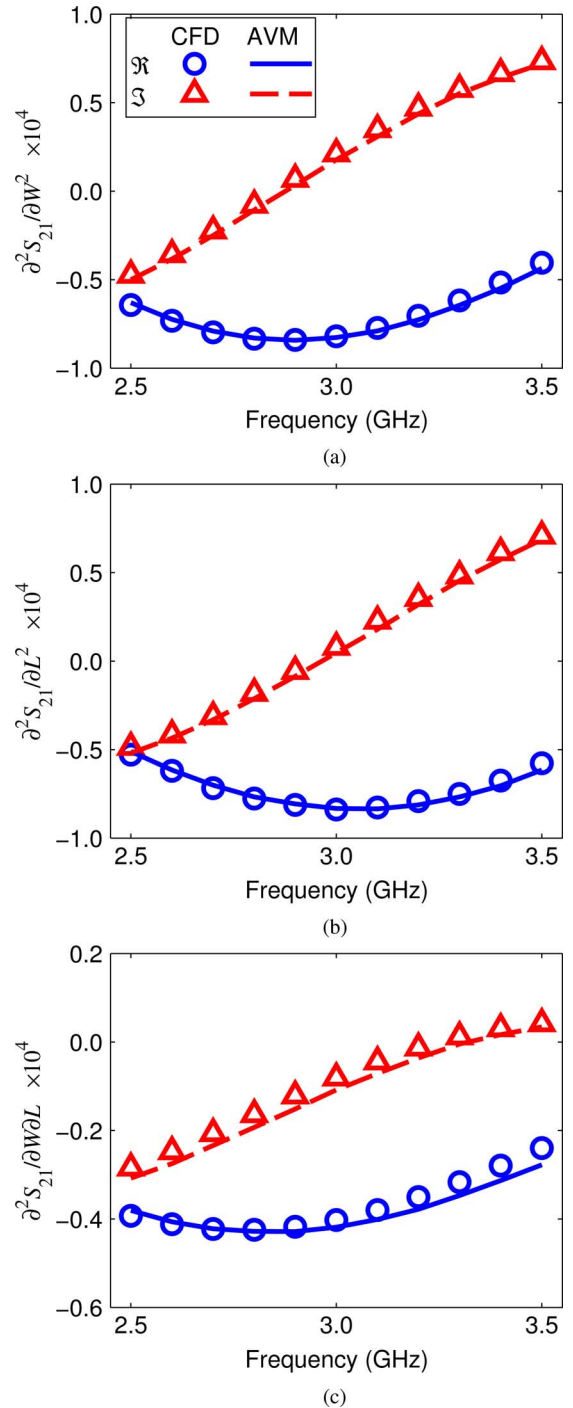


Fig. 7. Second-order sensitivities of the scattering parameters, with respect to length, L , and width, W , for the inductive obstacle example shown in Fig. 5. Sensitivities are computed by CFD, symbols, and AVM, lines, at different frequencies. Real part $\Re\{S_{21}\}$ (\circ , $—$) and imaginary $\Im\{S_{21}\}$ (Δ , $- - -$).

L . The results are shown in Fig. 6. Good agreement is achieved with CFD. The number of the required independent simulations has been reduced from 9 to only 4.

C. S-Parameters Sensitivities for the Inductive Obstacle

We demonstrate the estimation of the second-order sensitivities of the scattering parameters for the inductive obstacle example in Fig. 5. The vector of design parameters is $\mathbf{x} = [W L]^T$.

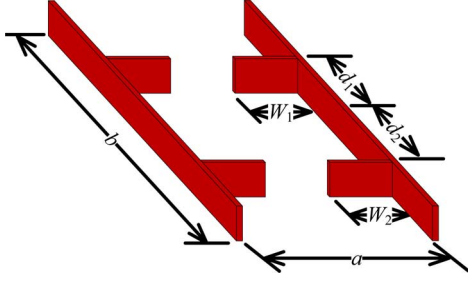


Fig. 8. 2-D single resonator filter of width $a = 60$ mm and length $b = 78$ mm. The TLM cell is $\Delta l = 1.0$ mm. The initial values for the filter parameters are $W_1 = W_2 = 8.0$ mm and $d_1 = d_2 = 18.0$ mm.

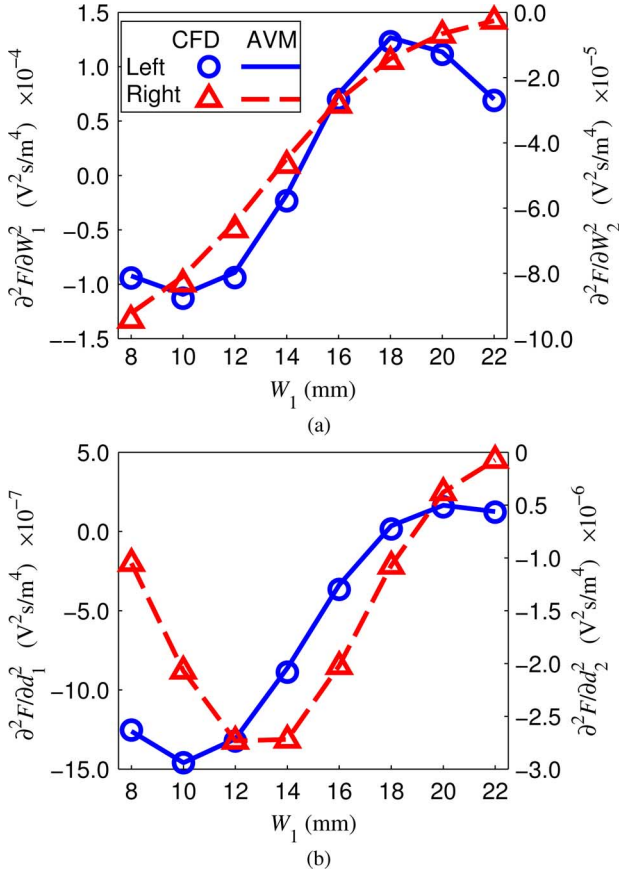


Fig. 9. Second-order sensitivities of the objective function in (22) with respect to W_1 , W_2 , d_1 , and d_2 , for the single resonator example shown in Fig. 8. The sensitivities are computed by CFD, \circ , \triangle , and AVM, — , --- . (a) $\partial^2 F / \partial W_1^2$ (left y-axis), $\partial^2 F / \partial W_2^2$ (right y-axis); and (b) $\partial^2 F / \partial d_1^2$ (left y-axis), $\partial^2 F / \partial d_2^2$ (right y-axis).

Our AVM approach is applied to estimate the wideband second derivative of the insertion loss, S_{21} , with respect to \mathbf{x} . The insertion loss is defined as the ratio between the output spectrum of the output port and the reference incident spectrum at the input port. The output spectrum of the desired mode at port 2 due to a sinusoidal excitation of frequency, f_0 , at port 1 is described as [25]

$$\tilde{\mathbf{E}}_{21}(f_0) = \int_0^{T_m} \int_{\text{Port2}} \int E(t, \mathbf{r}) E_2(\mathbf{r}) \exp(-j\omega t) ds dt \quad (23)$$

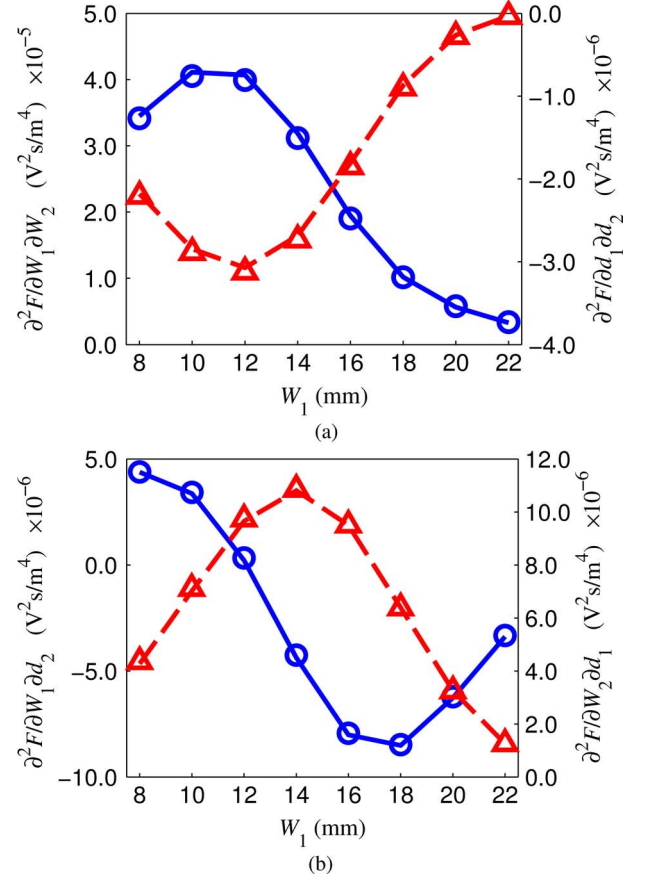


Fig. 10. Second-order sensitivities of the objective function in (22) with respect to W_1 , W_2 , d_1 , and d_2 , for the single resonator example shown in Fig. 8. The sensitivities are computed by CFD, \circ , \triangle , and AVM, — , --- . (a) $\partial^2 F / \partial W_1 \partial W_2$ (left y-axis), $\partial^2 F / \partial d_1 \partial d_2$ (right y-axis); and (b) $\partial^2 F / \partial W_1 \partial d_2$ (left y-axis), $\partial^2 F / \partial W_2 \partial d_1$ (right y-axis).

where \mathbf{r} denotes the position vector, $E_2(\mathbf{r})$ is the mode profile at the incident port (TE₁₀-mode), $E(t, \mathbf{r})$ is the electric field vector, $j = \sqrt{-1}$, and $\omega = 2\pi f_0$ is the angular frequency. The double integral is reduced to a single integral in this 2-D simulation. The time integral represents the Fourier transform. Using an approach similar to [25], the sensitivities of the real and imaginary parts of (23) is estimated. The results for wideband second-order sensitivity analysis of the real and imaginary parts of the scattering parameter are shown in Fig. 7. The results obtained with the proposed approach match the CFD estimates.

D. Single Resonator Filter

Next, we consider the single resonator waveguide filter shown in Fig. 8. It has a width $a = 60$ mm and a length $b = 78$ mm. Four metallic arms control the response of the filter. Each arm has a length W and resides at a distance d away from the waveguide center (see Fig. 8). Symmetry has been employed to simulate half of the domain. The filter is excited by a wideband Gaussian-modulated sine wave centered at 3.0 GHz with a bandwidth of 3.0 GHz. John's matrix [30] is utilized as a wideband absorbing boundary condition. The vector of design parameters is $\mathbf{x} = [W_1 \ W_2 \ d_1 \ d_2]^T$. The objective function is taken as the energy function (22). Figs. 9 and 10 show the sensitivity results. The proposed AVM method

TABLE I
SIMULATION TIME FOR CFD AND AVM

Parameter	CFD	AVM
Number of main function calls	21	6
CPU Time (s)	384	240
Memory Usage (MB) / simulation	685	352

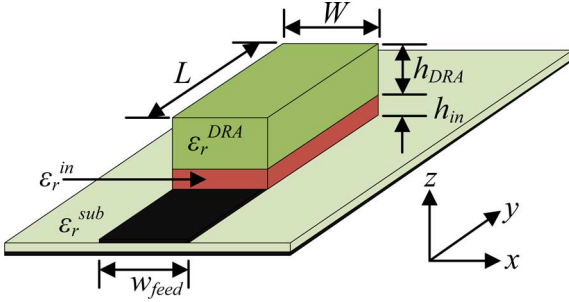


Fig. 11. 3-D DRA.

TABLE II
SUMMARY OF PARAMETERS FOR THE DRA

Parameter	Symbol	Value	Unit
Substrate relative permittivity	ϵ_r^{sub}	3.0	
Substrate height	h_{sub}	0.762	mm
Microstrip line width	w_{feed}	1.9	mm
Insert relative permittivity	ϵ_r^{in}	20.0	
Insert height	h_{in}	0.6	mm
DRA relative permittivity	ϵ_r^{DRA}	10.0	
DRA height	h_{DRA}	3.175	mm
DRA, insert length	L	7.875	mm
DRA, insert width	H	2.0	mm

successfully estimates the sensitivity of the objective function for eight different variables in reference to the CFD. The number of simulations has been reduced from 21 independent simulations—in the CFD case, down to only six simulations using AVM, i.e., 28%. Table I compares the CPU time and memory usage between AVM and CFD.

E. Dielectric Resonator Antenna (DRA) (3-D TLM)

The final example is a 3-D TLM DRA, as shown in Fig. 11 [31], [32]. The antenna is characterized by a wideband response, operating at a center frequency of 15 GHz with 8.0-GHz bandwidth. The antenna is fed by a microstrip line of width, w_{feed} . The substrate has a relative permittivity ϵ_r^{sub} and height, h_{sub} . The DRA radiating material has relative permittivity ϵ_r^{DRA} and dimensions L, W, h_{DRA} . A dielectric insert of relative permittivity ϵ_r^{in} and dimensions L, W , and h_{in} is placed between the microstrip feed line and the DRA. The insert expands the bandwidth of the antenna by enhancing the impedance matching over a wide band of frequencies. Table II shows the numeric values of the design parameters. The vector of design parameter is $\mathbf{x} = [\epsilon_r^{in}, \epsilon_r^{DRA}, h_{in}, h_{DRA}, L]$. The objective function is the return loss, S_{11} , defined as the ratio between the input spectrum of the input port and the reference incident spectrum at the input port.

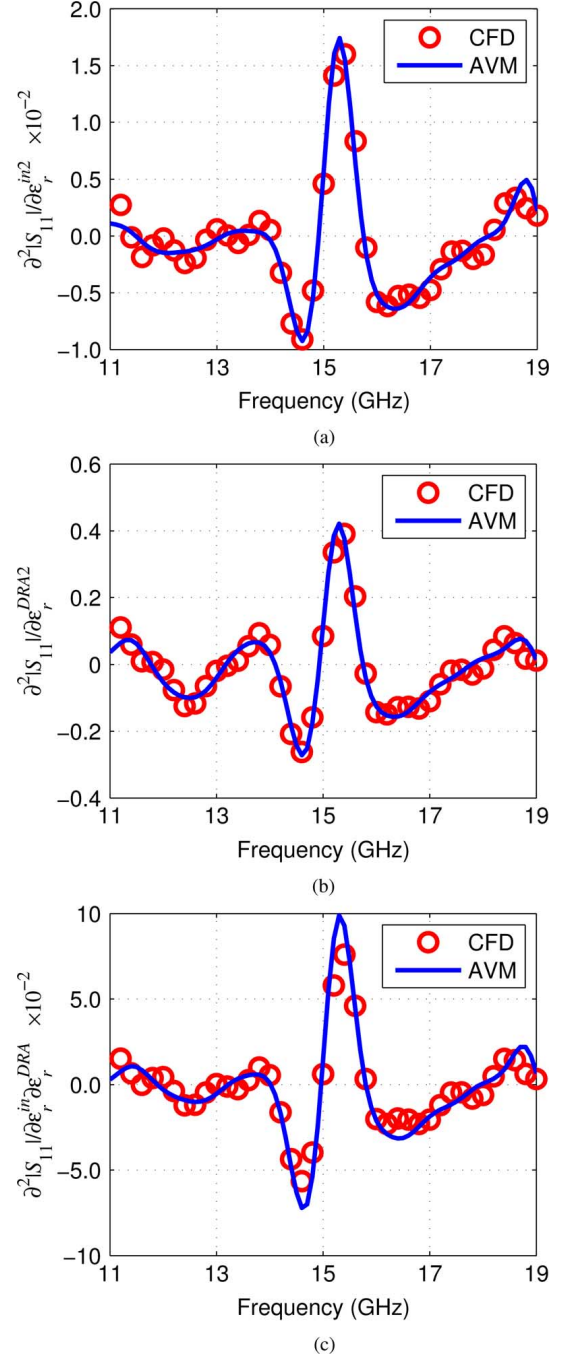


Fig. 12. Second-order sensitivities of the objective function in (24) with respect to ϵ_r^{in} and ϵ_r^{DRA} for DRA shown in Fig. 11. The sensitivities are computed by CFD, \circ , and AVM, $-$. (a) $\partial^2|S_{11}|/\partial\epsilon_r^{in^2}$, (b) $\partial^2|S_{11}|/\partial\epsilon_r^{DRA^2}$, and (c) $\partial^2|S_{11}|/\partial\epsilon_r^{in}\partial\epsilon_r^{DRA}$.

The input spectrum is given by

$$\tilde{\mathbf{E}}_{11}(f_0) = \int_0^{T_m} \int_{\text{Port1}} \int E(t, \mathbf{r}) E_1(\mathbf{r}) \exp(-j\omega t) ds dt \quad (24)$$

where $E_1(\mathbf{r})$ is the mode profile at the input port. Given the six design parameters in \mathbf{x} , a total of 21 sensitivities are estimated. Few are shown due to space limitation. The second-order sensitivities produced by our AVM approach in comparison with CFD is shown in Fig. 12 (for $\partial^2|S_{11}|/\partial\epsilon_r^{in^2}$, $\partial^2|S_{11}|/\partial\epsilon_r^{DRA^2}$,

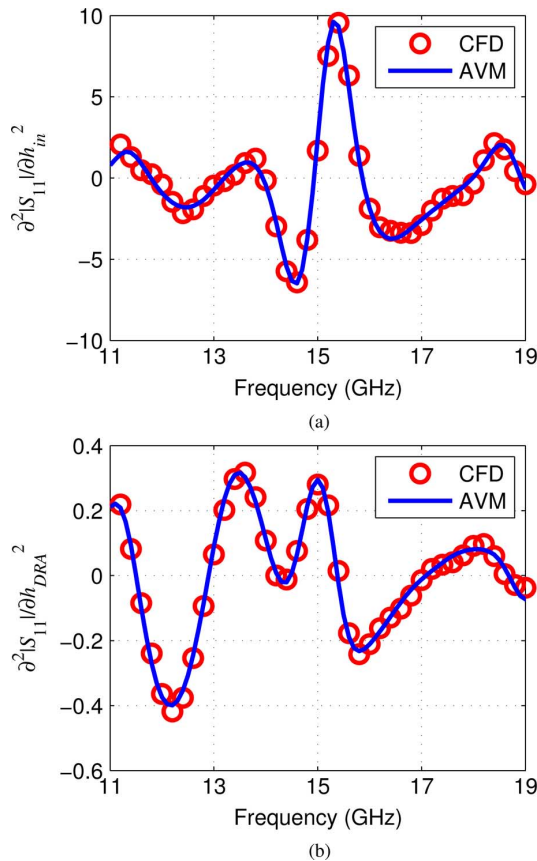


Fig. 13. Second-order sensitivities of the objective function in (24) with respect to ϵ_r^{in} and ϵ_r^{DRA} for DRA shown in Fig. 11. The sensitivities are computed by CFD, \circ , and AVM, —. (a) $\partial^2 |S_{11}| / \partial h_{in}^2$ and (b) $\partial^2 |S_{11}| / \partial h_{DRA}^2$.

and $\partial^2 |S_{11}| / \partial \epsilon_r^{\text{in}} \partial \epsilon_r^{\text{DRA}}$) and Fig. 13 (for $\partial^2 |S_{11}| / \partial h_{in}^2$ and $\partial^2 |S_{11}| / \partial h_{DRA}^2$). A good agreement is achieved.

VI. CONCLUSION

We have presented a new technique for estimating wideband second-order sensitivities for time-domain EM simulators. It is based on AVM, previously used for first-order response sensitivities [6]. This technique reduces the number of simulations from $O(n^2)$ to $O(n)$ when compared to finite-difference techniques. The accuracy of the proposed technique has been verified through a number of examples. Results from the proposed AVM technique match those estimated using CFDs. Two types of objective functions have been utilized including the energy function and the scattering parameters.

REFERENCES

- [1] J. W. Bandler and S. H. Chen, "Circuit optimization: The state of the art," *IEEE Trans. Microw. Theory Techn.*, vol. 36, no. 2, pp. 424–443, Feb. 1988.
- [2] P. Garcia and J. P. Webb, "Optimization of planar devices by the finite element method," *IEEE Trans. Microw. Theory Techn.*, vol. 38, no. 1, pp. 48–53, Jan. 1990.
- [3] Y. S. Chung, J. Ryu, C. Cheon, I. H. Park, and S. Y. Hahn, "Optimal design method for microwave device using time domain method and design sensitivity analysis. i. FETD case," *IEEE Trans. Magn.*, vol. 37, no. 5, pp. 3289–3293, Sep. 2001.

- [4] J. P. Webb, "Design sensitivities using high-order tetrahedral vector elements," *IEEE Trans. Magn.*, vol. 37, no. 5, pp. 3600–3603, Sep. 2001.
- [5] M. H. Bakr and N. K. Nikolova, "An adjoint variable method for frequency-domain TLM problems with conducting boundaries," *IEEE Microw. Wireless Compon. Lett.*, vol. 13, no. 9, pp. 408–410, Sep. 2003.
- [6] M. H. Bakr and N. K. Nikolova, "An adjoint variable method for time-domain transmission-line modeling with fixed structured grids," *IEEE Trans. Microw. Theory Techn.*, vol. 52, no. 2, pp. 554–559, Feb. 2004.
- [7] N. K. Nikolova, H. W. Tam, and M. H. Bakr, "Sensitivity analysis with the FDTD method on structured grids," *IEEE Trans. Microw. Theory Techn.*, vol. 52, no. 4, pp. 1207–1216, Apr. 2004.
- [8] E. A. Soliman, M. H. Bakr, and N. K. Nikolova, "An adjoint variable method for sensitivity calculations of multiport devices," *IEEE Trans. Microw. Theory Techn.*, vol. 52, no. 2, pp. 589–599, Feb. 2004.
- [9] HFSS. ANSYS, Canonsburg, PA, USA, Jul. 12, 2013. [Online]. Available: <http://www.ansys.com/hfss>
- [10] Computer Simulation Technology. CST, Framingham, MA, USA, Jul. 12, 2013. [Online]. Available: <http://www.cst.com>
- [11] J. Nocedal and S. J. Wright, *Numerical Optimization*. Berlin, Germany: Springer Verlag, 1999.
- [12] M. J. D. Powell, "Some global convergence properties of a variable metric algorithm for minimization without exact line searches," *Nonlinear Program.*, vol. 9, pp. 53–72, 1976.
- [13] R. Fletcher and M. J. D. Powell, "A rapidly convergent descent method for minimization," *Comput. J.*, vol. 6, no. 2, pp. 163–168, 1963.
- [14] C. G. Broyden, "The convergence of a class of double-rank minimization algorithms 2: The new algorithm," *IMA J. Appl. Math.*, vol. 6, no. 3, pp. 222–231, 1970.
- [15] E. J. Haug and P. E. Ehle, "Second-order design sensitivity analysis of mechanical system dynamics," *Int. J. Numer. Methods Eng.*, vol. 18, no. 11, pp. 1699–1717, 1982.
- [16] Z. Wang, I. M. Navon, F. X. Le Dimet, and X. Zou, "The second order adjoint analysis: Theory and applications," *Meteorol. Atmospher. Phys.*, vol. 50, no. 1–3, pp. 3–20, 1992.
- [17] J. W. Bandler and R. E. Seviiora, "Wave sensitivities of networks," *IEEE Trans. Microw. Theory Techn.*, vol. MTT-20, no. 2, pp. 138–147, Feb. 1972.
- [18] T. Redon and G. Vasilescu, "Second- and third-order sensitivities of microwave circuits," *Electron. Lett.*, vol. 25, no. 9, pp. 607–609, 1989.
- [19] M. A. E. Sabbagh, M. H. Bakr, and J. W. Bandler, "Adjoint higher order sensitivities for fast full-wave optimization of microwave filters," *IEEE Trans. Microw. Theory Techn.*, vol. 54, no. 8, pp. 3339–3351, Aug. 2006.
- [20] X. Ye, P. Li, and F. Y. Liu, "Exact time-domain second-order adjoint-sensitivity computation for linear circuit analysis and optimization," *IEEE Trans. Circuits Syst. I, Reg. Papers*, vol. 57, no. 1, pp. 236–248, Jan. 2010.
- [21] M. H. Negm, M. H. Bakr, and N. Nikolova, "Second-order time-domain adjoint sensitivity analysis exploiting TLM," in *IEEE MTT-S Int. Microw. Symp. Dig.*, 2012, pp. 1–3.
- [22] W. J. R. Hofer, "The transmission-line matrix method—Theory and applications," *IEEE Trans. Microw. Theory Techn.*, vol. MTT-33, no. 10, pp. 882–893, Oct. 1985.
- [23] P. B. Johns, "The solution of inhomogeneous waveguide problems using a transmission-line matrix," *IEEE Trans. Microw. Theory Techn.*, vol. MTT-22, no. 3, pp. 209–215, Mar. 1974.
- [24] M. H. Bakr and N. K. Nikolova, "An adjoint variable method for time-domain TLM with wideband Johns matrix boundaries," *IEEE Trans. Microw. Theory Techn.*, vol. 52, no. 2, pp. 678–685, Feb. 2004.
- [25] M. H. Bakr and N. K. Nikolova, "Efficient estimation of adjoint-variable S -parameter sensitivities with time domain TLM," *Int. J. Numer. Model.*, vol. 18, no. 2, pp. 171–187, 2005.
- [26] M. H. Bakr, N. K. Nikolova, and P. A. W. Basl, "Self-adjoint S -parameter sensitivities for lossless homogeneous TLM problems," *Int. J. Numer. Model.*, vol. 18, no. 6, pp. 441–455, 2005.
- [27] P. A. W. Basl, M. H. Bakr, and N. K. Nikolova, "Efficient estimation of sensitivities in TLM with dielectric discontinuities," *IEEE Microw. Wireless Compon. Lett.*, vol. 15, no. 2, pp. 89–91, Feb. 2005.
- [28] M. Abramowitz and I. A. Stegun, *Handbook of Mathematical Functions with Formulas, Graphs, and Mathematical Tables*, 9th ed. New York, NY, USA: Dover, 1964.
- [29] O. S. Ahmed, M. H. Bakr, and X. Li, "A memory-efficient implementation of TLM-based adjoint sensitivity analysis," *IEEE Trans. Antennas Propag.*, vol. 60, no. 4, pp. 2122–2125, Apr. 2012.

- [30] N. K. Eswarappa, G. I. Costache, and W. J. R. Hoefer, "Transmission line matrix modeling of disperse wideband absorbing boundaries with time-domain diakoptics for S -parameter extraction," *IEEE Trans. Microw. Theory Techn.*, vol. 38, no. 4, pp. 379–386, Apr. 1990.
- [31] A. Petosa, N. Simons, R. Siushansian, A. Ittipiboon, and M. Cuhaci, "Design and analysis of multisegment dielectric resonator antennas," *IEEE Trans. Antennas Propag.*, vol. 48, no. 5, pp. 738–742, May 2000.
- [32] O. S. Ahmed, M. H. Bakr, and X. Li, "An impulse sampling approach for efficient 3-D TLM-based adjoint sensitivity analysis," *Prog. Electromagn. Res.*, vol. 142, pp. 485–503, 2013.



Mohamed H. Negm (S'06) was born in Giza, Egypt, in 1982. He received the B.Sc. degree (with honors) in biomedical engineering from Cairo University, Giza, Egypt, in 2005, the M.A.Sc. degree in biomedical engineering from McMaster University, Hamilton, ON, Canada, in 2008, and is currently working toward his Ph.D. degree in electrical and computer engineering at McMaster University.

From 2005 to 2006, he became an Electronic Design Engineer with BMA for Design and Industry, Giza, Egypt. He then joined the Electrical and Com-

puter Engineering Department, McMaster University, where he is currently a member of the Computational Electromagnetics Laboratory. His research interests include antenna design for medical applications, optimization, embedded design, digital and analog electronics, and physiological modeling.

Mr. Negm was the recipient of Ontario (OGS) and Ann Poucher Windsor Queen Elizabeth II graduate scholarships.



Mohamed H. Bakr (S'98–M'00–SM'10) received the B.Sc. degree in electronics and communications engineering [with distinction (honors)] and Masters degree in engineering mathematics from Cairo University, Giza, Egypt, in 1992 and 1996, respectively, and the Ph.D. degree in electrical and computer engineering from McMaster University, Hamilton, ON, Canada, in 2000.

In 1997, he was a Student Intern with Optimization Systems Associates (OSA) Inc. From 1998 to 2000, he was a Research Assistant with the Simulation Optimization Systems (SOS) Research Laboratory, McMaster University. In November 2000, he joined the Computational Electromagnetics Research Laboratory (CERL), University of Victoria, Victoria, BC, Canada, as a Natural Sciences and Engineering Research Council of Canada (NSERC) Post-Doctoral Fellow. He is currently a Professor with the Department of Electrical and Computer Engineering, McMaster University. His research interests include optimization methods, computer-aided design (CAD) and modeling of microwave circuits and photonic devices, neural network applications, smart analysis of high-frequency structures, and efficient optimization using time/frequency-domain methods.

Dr. Bakr was the recipient of a Premier's Research Excellence Award (PREA) of the Province of Ontario, Canada (2003) and a National Science and Engineering Research Council (NSERC) of Canada Discovery Accelerator Supplements (DAS) Award (2011).



Osman S. Ahmed (S'10–M'13) received the B.Sc. degree in electronics and communications engineering [with distinction (honors)] and M.Sc. degree in engineering physics from Cairo University, Giza, Egypt, in 2005 and 2009, respectively, and the Ph.D. degree electrical and computer engineering from McMaster University, Hamilton, ON, Canada, in 2013.

From 2009 to 2013, he was a Research Assistant with the Computational Electromagnetics Research Laboratory (CEML), McMaster University. In September 2013, he joined the Department of Electrical and Computer Engineering, University of Toronto, Toronto, ON, Canada as a Natural Sciences and Engineering Research Council (NSERC) of Canada Post-Doctoral Fellow. His research areas include design optimization of nano-plasmonic devices, optical interconnects, plasmonic bio-sensors, biophotonics, and terahertz spectroscopy.

Dr. Ahmed was a recipient of the Clifton W. Sherman Scholarship (2010) for doctoral studies in science and engineering from McMaster University, the Ontario Graduate Scholarship (OGS) Award (2012), and the NSERC of Canada Post Doctoral Fellowship (2013).



Natalia K. Nikolova (S'93–M'97–SM'05–F'11) received the Dipl. Eng. degree from the Technical University of Varna, Varna, Bulgaria, in 1989, and the Ph.D. degree from the University of Electro-Communications, Tokyo, Japan, in 1997.

From 1998 to 1999, she held a Postdoctoral Fellowship with the Natural Sciences and Engineering Research Council (NSERC) of Canada, during which time she was initially with the Microwave and Electromagnetics Laboratory, DalTech, Dal-

housie University, Halifax, NS, Canada, and later, for a year, with the Simulation Optimization Systems Research Laboratory, McMaster University, Hamilton, ON, Canada. In July 1999, she joined the Department of Electrical and Computer Engineering, McMaster University, where she is currently a Professor. Her research interests include theoretical and computational electromagnetism, inverse scattering, and microwave imaging, as well as methods for the computer-aided analysis and design of microwave structures and antennas. Since 2008, she has been a Canada Research Chair in High-frequency Electromagnetics.

Dr. Nikolova is currently a Distinguished Microwave Lecturer. She is a member of the Applied Computational Electromagnetics Society (ACES) and a correspondent of the International Union of Radio Science (URSI). She was the recipient of a University Faculty Award of the NSERC (2000–2005).



John W. Bandler (S'66–M'66–SM'74–F'78–LF'06) studied at the Imperial College of Science and Technology, London, U.K. He received the B.Sc. (Eng.), Ph.D., and D.Sc. (Eng.) degrees from the University of London, London, U.K., in 1963, 1967, and 1976, respectively.

In 1969, he joined McMaster University, Hamilton, ON, Canada. He is currently a Professor Emeritus with McMaster University. In 1983, he founded Optimization Systems Associates Inc., and in 1997, sold it to the Hewlett-Packard Company. In 1997, he founded Bandler Corporation. He has authored or coauthored over 480 technical papers.

Dr. Bandler is a Fellow of several societies, including the Canadian Academy of Engineering and the Royal Society of Canada (since 1986). He has served on Editorial Boards and Technical Program Committees as a guest editor. He was the recipient of the IEEE Microwave Theory and Techniques Society (IEEE MTT-S) 2004 Microwave Application Award and the IEEE Canada 2012 A. G. L. McNaughton Gold Medal. He was a recipient of the 2012 Queen Elizabeth II Diamond Jubilee Medal. For his lifetime achievements in the field of microwave theory and techniques, he received the IEEE MTT-S 2013 Microwave Career Award.